An LMI-Based Linear Quadratic Regulator (LQR) Control for Modular Multilevel Converters (MMCs) Considering Parameters Uncertainty

Homa Sheikhi Jouybary, Augustin Mpanda Mabwe, Davood Arab Khaburi, Ahmed El Hajjaji

IEEE Access
Multidisciplinary | Rapid Review | Open Access Journal

IEEE POWER & ENERGY SOCIETY SECTION

Received 19 July 2024, accepted 2 August 2024, date of publication 12 August 2024, date of current version 21 August 2024.

Digital Object Identifier 10.1109/ACCESS.2024.3442090

RESEARCH ARTICLE

An LMI-Based Linear Quadratic Regulator (LQR) Control for Modular Multilevel Converters (MMCs) Considering Parameters Uncertainty

HOMA SHEIKHI JOUYBARY[1,2], (Student Member, IEEE), AUGUSTIN MPANDA MABWE[3], (Senior Member, IEEE), DAVOOD ARAB KHABURI[1], AND AHMED EL HAJJAJI[2]

[1]School of Electrical Engineering, Iran University of Science and Technology, Tehran 16846-13114, Iran
[2]MIS Laboratory, University of Picardie Jules Verne, 80039 Amiens, France
[3]SYMADE, UniLaSalle Polytechnic Institute, 80082 Amiens, France

Corresponding author: Homa Sheikhi Jouybary (homa.sheikhi@yahoo.com)

This work was supported in part by the Hauts-de-France (HDF) region, and in part by the Ministry of Science, Research and Technology (MSRT) of Iran.

ABSTRACT This paper presents the robust linear quadratic regulator (LQR) control for the uncertain modular multilevel converters (MMCs). The classical LQR control prioritizes optimizing the performance index but lacks the ability to address converter uncertainties. This paper takes into account this limitation by developing a model of the MMC that considers parameter uncertainties. To enable LQR control in uncertain MMC systems, an optimization approach for the performance index employing linear matrix inequality (LMI) technique is proposed. Consequently, a novel robust control strategy for MMCs is established. The real-time performance of this LMI-based LQR control is evaluated against classical LQR control under both nominal and non-nominal conditions and single phase-to-ground fault using Opal-RT system. For this purpose, as the switching function model sufficiently captures all aspects of the MMC's behavior, the switching function model of the MMC is implemented on the Opal-RT OP4610XG system for real-time emulation of MMC. The results from real-time simulation of the system indicate that the proposed LMI-LQR method offers an advantage in robustness over the classical LQR method in presence of parameters uncertainty.

INDEX TERMS Linear matrix inequality (LMI), linear quadratic regulator (LQR), modular multilevel converter (MMC, M2C), parameters uncertainty, real-time emulated MMC model, real-time simulation, robust control.

I. INTRODUCTION

In recent years, there has been growing interest in modular multilevel converters (MMCs), positioning them as prominent converter configurations for medium and high voltage applications. The key features of the MMC include [1] and [2]: (i) scalability to different power and voltage levels due to their modular structure, (ii) providing high-quality output voltages due to potential to generate higher number of voltage levels, thereby reducing filtering needs, (iii) high efficiency, (iv) no need for a usual DC-bus capacitor, and (v) redundant configuration. Due to its numerous advantages, the MMC is highly appropriate for applications involving grid connection, such as high-voltage direct-current (HVDC) transmission systems [3], static synchronous compensators (STATCOMs) [4], renewable energy conversion systems [5] and [6], battery energy storage systems (BESS) [7], and etc.

Although MMCs provide several advantages, their control presents greater complexity and challenge compared to conventional voltage source converters (VSCs). This complexity

The associate editor coordinating the review of this manuscript and approving it for publication was Santu Giri.

stems from the presence of multiple control objectives that must be satisfied concurrently. Indeed, besides regulating AC-side power/current, it is essential to simultaneously control circulating currents and submodule (SM) capacitor voltages [8]. Various control strategies for MMCs have been proposed in the literature to enhance control performance. The designed MMC controller should prioritize simplicity and ease of implementation. In this context, the linear quadratic regulator (LQR) as an optimal control technique emerges as a promising choice for controlling the MMC [9].

In [9], a linear quadratic regulator involving integral action is presented to achieve a specified level of stability of MMC by relocating the closed-loop poles. The LQR control for MMCs in [10], emphasizes high performance through optimal quadratic cost minimization, with a simplified control structure. In [11], an approach utilizing Piecewise LQR is proposed for optimizing current and energy control, and energy balancing within MMCs. The research work in [12] utilized a robust control approach for the MMC-HVDC, called the optimal guaranteed cost method. This approach involves designing a controller that optimizes a guaranteed cost criterion subject to system uncertainties and constraints. In many studies, the LQR controller is obtained by solving an algebraic Riccati equation (ARE). However, it is worth noting that the LQR problem can be expressed in terms of linear matrix inequalities (LMIs) and solved by using convex optimization methods [13] and [14].

Moreover, data-driven approaches such as reinforcement learning (RL) has recently emerged as appealing subject in the design of adaptive optimal controllers [15], as they enable the design of controllers without prior knowledge of the system and can automatically adapt to changing system characteristics (self-adaptiveness) [16]. For instance, the [15] presented an adaptive dynamic programming control using critic neural network (NN) for robust predictive control of MMCs. In [16], a conventional RL algorithm is used by integrating constrained optimal control and online model identification to achieve safe RL and a model-free controller design in a three-level voltage source inverter for applications in islanded power grids. Afterward, [17] presented a RL-based control approach for buck converters, eliminating the need for an accurate system model by utilizing measured data to solve an optimization problem derived from the LQR and involves solving an ARE iteratively. Despite these advances, designing RL-based optimal controllers is complicated by practical challenges such as parametric uncertainties and external disturbances [15].

The classical LQR control [10] and [18], focuses on optimizing a cost function or performance index. The LQR framework ensures that solving the algebraic Riccati equation yields an optimal converter system. However, it is incapable of addressing converter system uncertainty. Neglecting uncertainty in parameters of the system in a design may lead to degraded output signal or instability when faced with significant disturbances [13]. To address parameters uncertainty, this paper introduces a simple state-feedback controller utilizing an LMI-based LQR approach, which enables the achievement of robust stability and performance even in the presence of parameters uncertainty.

This study adopts the use of the classic LQR method as a basis for adjusting controller gains, which can be expressed as a performance-based optimization problem. Numerical solution techniques and software tools for solving such problems are readily accessible [19]. This strategy can take into account uncertain parameters in the MMC system by incorporating variations in these parameters within a bounded set in the nominal model matrices [20]. Another advantage is that it can simultaneously incorporate multiple design requirements, such as pole placement [21] and input constraints as in [20]. Concisely, this method enables the integration of the characteristics of LQR control with uncertainty and other criteria.

Furthermore, this paper contribution involves the introduction of LQR control for MMC utilizing LMI and solving it through convex optimization methods. This approach adapts an LMI formulation of the LQR problem from [14]. The subsequent sections are structured as follows: Section II presents the mathematical model of the uncertain MMC. Section III elaborates on the formulation of the LQR problem using LMI, followed by the overall control strategy for MMC. Section IV presents the digital real-time simulation results. Finally, Section V summarizes the conclusion.

II. MATHEMATICAL MODEL OF THE UNCERTAIN MMC

The three-phase MMC structure is configured by connecting N identical half-bridge submodules (HB-SMs) in series within each arm, as shown in Fig. 1. The MMC consists of three legs, with each leg comprises both upper (u) and lower (l) arms. Each submodule includes a DC energy storage capacitor (C), two controllable semiconductor devices, and two anti-parallel diodes, creating a bidirectional HB-SM. Each SM can switch between *insert* and *bypass* states. In the *insert* state, the upper switch of SM (S_i) conducts, and the SM voltage (v_{SM_i}) equals the SM capacitor voltage (v_{c_i}). In contrast, in the *bypass* state, the lower switch of SM ($\bar{S}_i$) conducts, resulting in no current circulation through the capacitor and a zero SM voltage. Therefore, the voltage across the arbitrary ith submodule, from either the upper or lower arms of arbitrary phase can be represented as:

$$v_{SM_i} = S_i v_{c_i} \tag{1}$$

where, the S_i is the switching state of the upper switch of submodule i, where i is the SM identifier, defined as:

$$S_i = \begin{cases} 1 & \textit{insert mode} \\ 0 & \textit{bypass mode} \end{cases} \tag{2}$$

In each arm, an inductor (L) is employed to reduce arm current harmonics and to restrict the fault current. Additionally, an equivalent arm resistor (R) is incorporated to account for losses arising from various factors, such as semiconductors, the equivalent series resistance in the SM capacitor, and the arm inductor, etc.

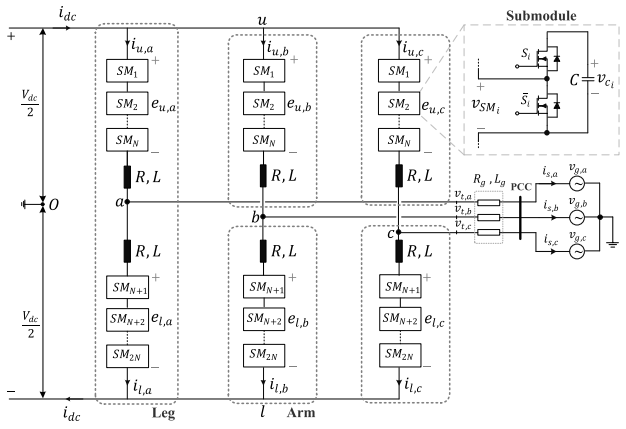

FIGURE 1. The structure of three-phase grid-connected MMC.

The DC-bus voltage, identified as V_{dc}, connects the u and l points, while i_{dc} stand for the DC-bus current. The currents passing through the upper and lower arms in three phases are denoted as $i_{u,a}$, $i_{l,a}$, $i_{u,b}$, $i_{l,b}$, $i_{u,c}$, and $i_{l,c}$. On the other hand, the voltages generated by the upper and lower arms in three phases are represented by $e_{u,a}$, $e_{l,a}$, $e_{u,b}$, $e_{l,b}$, $e_{u,c}$, and $e_{l,c}$. The terminal of MMC is connected to an ideal AC grid in the point of common coupling (PCC) by means of AC filter with MMC terminal AC voltages are $v_{t,a}$, $v_{t,b}$, and $v_{t,c}$, while the three-phase grid voltages are $v_{g,a}$, $v_{g,b}$, and $v_{g,c}$.

In each arm of MMC, the voltage at the terminal of the series connected SMs can be considered as a controlled voltage source. Thereby the MMC can be represented with six controlled voltage sources [22]. The average model/conrol of MMCs is frequently enabled by separating the high-level control system from the low-level control. For each arm, the low-level control system facilitates the conversion of a specified reference voltage determined by high-level control into switching signals for the SMs, while ensuring the balance of capacitor voltages within each arm. Accordingly, the MMC can be modeled at a higher level, simplifying the modeling process and considers only the currents (phase/circulating) dynamics [10] and [23], as applied in this paper.

The AC-side phase currents ($i_{s,j}$) for phase $j = a, b, c$, where j is the phase identifier, can be achieved through:

$$i_{s,j} = i_{u,j} - i_{l,j} \tag{3}$$

The circulating currents ($i_{c,j}$) are defined as (4):

$$i_{c,j} = \frac{i_{u,j} + i_{l,j}}{2} \tag{4}$$

Applying KVL on the upper and lower arm of each phase in Fig. 1, allows the equations for upper and lower arm voltages with respect to the DC-bus virtual midpoint (O) to be derived, as described in equations (5) and (6) respectively.

$$e_{u,j} = \frac{V_{dc}}{2} - L\frac{di_{u,j}}{dt} - Ri_{u,j} - v_{t,j} \tag{5}$$

$$e_{l,j} = \frac{V_{dc}}{2} - L\frac{di_{l,j}}{dt} - Ri_{l,j} + v_{t,j} \tag{6}$$

where, $e_{u,j}$ and $e_{l,j}$ denote arm output voltage. Adding and subtracting equations (5) and (6), along with the integration of equations (3) and (4), yield a new set of equations as given in (7) and (8).

$$\frac{L}{2}\frac{di_{s,j}}{dt} = -\frac{R}{2}i_{s,j} - v_{t,j} + \underbrace{\frac{-e_{u,j} + e_{l,j}}{2}}_{v_{s,j}} \tag{7}$$

$$L\frac{di_{c,j}}{dt} = -Ri_{c,j} + \underbrace{\frac{V_{dc} - e_{u,j} - e_{l,j}}{2}}_{v_{c,j}} \tag{8}$$

Given that $v_{t,j} = R_g i_{s,j} + L_g di_{s,j}/dt + v_{g,j}$ and by introducing $R_{eq} = R_g + R/2$ and $L_{eq} = L_g + L/2$, equation (7) can be reformulated in a simplified form, resulting in:

$$L_{eq}\frac{di_{s,j}}{dt} = -R_{eq}i_{s,j} + v_{s,j} - v_{g,j} \tag{9}$$

The single-phase model outlined in (9) and (8) can be extended to form a three-phase model, as in (10) and (11).

$$L_{eq}\frac{di_{s,abc}}{dt} = -R_{eq}i_{s,abc} + v_{s,abc} - v_{g,abc} \tag{10}$$

$$L\frac{di_{c,abc}}{dt} = -Ri_{c,abc} + v_{c,abc} \tag{11}$$

Utilizing the sine-based Park's transformation (the rotating frame is aligned 90 degrees behind the phase a axis) rotating at $+\omega$, the AC-side phase current in the dq-frame is calculated as follows:

$$L_{eq}\frac{di_{ds}}{dt} - \omega L_{eq}i_{qs} = -R_{eq}i_{ds} + \underbrace{v_{ds} - v_{dg}}_{v_d} \tag{12}$$

$$L_{eq}\frac{di_{qs}}{dt} + \omega L_{eq}i_{ds} = -R_{eq}i_{qs} + \underbrace{v_{qs} - v_{qg}}_{v_q} \tag{13}$$

The AC-side currents and the circulating currents are the most important control variables for an MMC. Thus, by choosing the state vector $x \in R^5 = [i_{ds} \quad i_{qs} \quad i_{c,j}^T]^T$, $i_{c,j}^T = [i_{c,a} \quad i_{c,b} \quad i_{c,c}]$ and the input vector $u \in R^5 = [v_d \quad v_q \quad v_{c,j}^T]^T$, $v_{c,j}^T = [v_{c,a} \quad v_{c,b} \quad v_{c,c}]$ according to (11), (12) and (13) the state-space model can be described as follows:

$$\begin{cases} \dot{x}_{(5\times1)} = A_{(5\times5)}x_{(5\times1)} + B_{(5\times5)}u_{(5\times1)} \\ y_{(5\times1)} = C_{(5\times5)}x_{(5\times1)} \end{cases}$$

$$A = \begin{pmatrix} -\frac{R_{eq}}{L_{eq}} & +\omega & 0 & 0 & 0 \\ -\omega & -\frac{R_{eq}}{L_{eq}} & 0 & 0 & 0 \\ 0 & 0 & -\frac{R}{L} & 0 & 0 \\ 0 & 0 & 0 & -\frac{R}{L} & 0 \\ 0 & 0 & 0 & 0 & -\frac{R}{L} \end{pmatrix},$$

$$B = \begin{pmatrix} \frac{1}{L_{eq}} & 0 & 0 & 0 & 0 \\ 0 & \frac{1}{L_{eq}} & 0 & 0 & 0 \\ 0 & 0 & \frac{1}{L} & 0 & 0 \\ 0 & 0 & 0 & \frac{1}{L} & 0 \\ 0 & 0 & 0 & 0 & \frac{1}{L} \end{pmatrix}. \quad (14)$$

where $A \in R^{5\times5}$, $B \in R^{5\times5}$, $C \in R^{5\times5} = I_5$.

The state-space model of the MMC is augmented by incorporating additional state variables, denoted as ξ. These variables represent the integral of the output error to ensure the steady-state error converges to zero.

$$\dot{\xi} = y^* - y = y^* - Cx \quad (15)$$

where, the symbol $*$ represents the related reference. Therefore, by introducing the augmented state vector $x_a = [x^T \quad \xi^T]^T$, the expression for the augmented state-space model is as (16).

$$\begin{cases} \dot{x}_{a(10\times1)} = A_{a(10\times10)} x_{a(10\times1)} + B_{a(10\times5)} u_{a(5\times1)} + r_{(10\times1)} \\ y_{(5\times1)} = C_{a(5\times10)} x_{a(10\times1)} \end{cases} \quad (16)$$

where:

$$A_a = \begin{bmatrix} A & 0_{5\times5} \\ -C & 0_{5\times5} \end{bmatrix}, \; B_a = \begin{bmatrix} B \\ 0_{5\times5} \end{bmatrix}, \; C_a = [C \quad 0_{5\times5}],$$

$$u_a = u, \; x_a = [x^T \quad \xi^T]^T, \; \xi = \begin{bmatrix} \xi_{ds} & \xi_{qs} & \xi_{c,j}^T \end{bmatrix}^T,$$

$$\xi_{ds} = \int (i_{ds}^* - i_{ds})dt, \; \xi_{qs} = \int (i_{qs}^* - i_{qs})dt,$$

$$\xi_{c,j} = \int (i_{c,j}^* - i_{c,j})dt, \; r = \begin{bmatrix} 0_{1\times5} & y^{*T} \end{bmatrix}^T.$$

Elements within the system matrices A and B, may exhibit uncertainty or vary over time. A dynamic model of the system is referred to as polytopic model when its matrices contain elements that exhibit linear dependency on uncertain parameters that vary within a bounded set [20]. Thus, (16) can be represented as a function of these parameters as:

$$\dot{x}_a = A_a(\rho)x_a + B_a(\rho)u_a \quad (17)$$

where, ρ is a vector consisting of n_p uncertain parameters $\rho = [\rho_1, \ldots, \rho_{n_p}]$, with each uncertain parameter ρ_i bounded between minimum (ρ_i^{min}) and maximum (ρ_i^{max}) values. Generally, the range of values for the vector ρ forms a convex polytope with $\mathcal{L} = 2^{n_p}$ vertices $\{v_1, \ldots, v_{\mathcal{L}}\}$.

In this paper, the considered uncertainties pertain to the arm resistance and inductance. We also assume that all other parameters are known. Therefore, the model for the MMC will be derived in terms of these two parameters. The vector of uncertain parameters is defined as $\rho = [R \; L]$ with the number of vertices of the polytope $\mathcal{L} = 2^2 = 4$, bounded by the minimum and maximum values as:

$$R \in \begin{bmatrix} R^{min} & R^{max} \end{bmatrix}, \quad L \in \begin{bmatrix} L^{min} & L^{max} \end{bmatrix} \quad (18)$$

The four vertices of polytopic model for matrices A_a and B_a can be defined such that the values of R and L depend on vertex of polytopic model as follows:

$$\begin{bmatrix} R^{min} & L^{min} \end{bmatrix} \in A_{a_1}, B_{a_1}$$
$$\begin{bmatrix} R^{min} & L^{max} \end{bmatrix} \in A_{a_2}, B_{a_2}$$
$$\begin{bmatrix} R^{max} & L^{min} \end{bmatrix} \in A_{a_3}, B_{a_3}$$
$$\begin{bmatrix} R^{max} & L^{max} \end{bmatrix} \in A_{a_4}, B_{a_4} \quad (19)$$

where, $B_{a_3} = B_{a_1}$ and $B_{a_4} = B_{a_2}$. This augmented polytopic model will be employed in next section to develop an LQR controller aimed at stabilizing the MMC despite uncertainties in the parameters of arm resistance and inductance using LMI formulations.

III. DESIGNING THE CONTROL SYSTEM FOR THE MMC

A. FORMULATING THE LQR PROBLEM USING LMI

In the system described in (17), the optimal LQR controller is derived by finding a control law by state-feedback $u_a = -Kx_a$ that minimizes the performance index in (20).

$$J = \int_0^\infty \left(x_a^T Q x_a + u_a^T R u_a \right) dt \quad (20)$$

where, Q represents the state weighting matrix, which is symmetric and positive semidefinite diagonal matrix. On the other hand, R denotes the control weighting matrix, which is symmetric and positive definite diagonal matrix. The performance index (20) in the closed loop can be expressed as:

$$J = \int_0^\infty \left(x_a^T \left(Q + K^T R K \right) x_a \right) dt \quad (21)$$

By employing the trace operator $Tr(\cdot)$, which is defined to be the sum of all elements of main diagonal of a matrix, and according to cyclic property of the trace, $Tr\left(x_a^T \left(Q + K^T R K\right) x_a\right) = Tr\left(\left(Q + K^T R K\right) x_a x_a^T\right)$, the performance index is equivalent to:

$$\begin{aligned} J &= \int_0^\infty Tr\left(\left(Q + K^T R K \right) x_a x_a^T \right) dt \\ &= Tr\left(\left(Q + K^T R K \right) P \right) \end{aligned} \quad (22)$$

where, $P = \int_0^\infty x_a x_a^T dt$ is a positive definite symmetric matrix that satisfies (23).

$$\begin{aligned} \left(A_{a_\ell} - B_{a_\ell} K\right) P + P(A_{a_\ell} - B_{a_\ell} K)^T + I = 0 \\ \ell = 1, \ldots, \mathcal{L} \end{aligned} \quad (23)$$

Then, (22) can be rewritten as:

$$\begin{aligned} J &= Tr\left(\left(Q + K^T R K \right) P \right) \\ &= Tr\left(QP \right) + Tr\left(K^T R K P \right) \end{aligned} \quad (24)$$

By utilizing cyclic property of the trace, the second term in (24) can be expressed as:

$$Tr\left(K^T R K P \right) = Tr\left(K P K^T R \right) = Tr\left(R^{\frac{1}{2}} K P K^T R^{\frac{1}{2}} \right) \quad (25)$$

Thereby, the optimal feedback gain K can be obtained by solving the minimization problem of the expression in (26).

$$\begin{aligned} &\min_{P,K} \; Tr\,(QP) + Tr\left(R^{\frac{1}{2}} K P K^T R^{\frac{1}{2}}\right) \\ &\text{subject to: } \left(A_{a_\ell} - B_{a_\ell} K\right) P + P(A_{a_\ell} - B_{a_\ell} K)^T + I < 0 \end{aligned} \tag{26}$$

Since (26) involves the multiplication of variables P and K, it is not linear. Therefore, to address this, a new variable $Y = KP$ is introduced, and (26) is reformulated as (27).

$$\begin{aligned} &\min_{P,Y} \; Tr\,(QP) + Tr\left(R^{\frac{1}{2}} Y P^{-1} Y^T R^{\frac{1}{2}}\right) \\ &\text{subject to: } A_{a_\ell} P + P A_{a_\ell}^T - B_{a_\ell} Y - Y^T B_{a_\ell}^T + I < 0 \end{aligned} \tag{27}$$

The nonlinear term $R^{\frac{1}{2}} Y P^{-1} Y^T R^{\frac{1}{2}}$ can be substituted with a second auxiliary variable X such that $X > R^{\frac{1}{2}} Y P^{-1} Y^T R^{\frac{1}{2}}$, which can be decomposed by Schur's complement.

$$X > R^{\frac{1}{2}} Y P^{-1} Y^T R^{\frac{1}{2}} \Longleftrightarrow \begin{bmatrix} X & R^{\frac{1}{2}} Y \\ Y^T R^{\frac{1}{2}} & P \end{bmatrix} > 0 \tag{28}$$

Therefore, the comprehensive LMI formulation of the LQR problem can be expressed as follows:

$$\begin{aligned} &\min_{P,Y,X} \; Tr\,(QP) + Tr\,(X) \\ &\text{subject to: } P > 0 \\ &\qquad A_{a_\ell} P + P A_{a_\ell}^T - B_{a_\ell} Y - Y^T B_{a_\ell}^T + I < 0 \\ &\qquad \ell = 1, \ldots, \mathcal{L} \\ &\qquad \begin{bmatrix} X & R^{\frac{1}{2}} Y \\ Y^T R^{\frac{1}{2}} & P \end{bmatrix} > 0 \end{aligned} \tag{29}$$

After solving this constrained minimization, the optimal LQR controller can be obtained by $K = YP^{-1}$. The obtained augmented gain matrix $K_{(5\times10)}$ is divided into two parts: $K_{P(5\times5)}$, representing the proportional matrix, and $K_{I(5\times5)}$, which corresponds to the integral action, such that $K = [K_P \quad K_I]$.

The merit of formulating the classical LQR problem as a convex optimization challenge lies in its ability to consider uncertainty, unlike classical LQR control which is restricted to systems without uncertainty.

B. ARM REFERENCE MODULATING SIGNALS CALCULATION

Two upper and lower arms reference modulating signals are produced by the MMC's high-level control system known as $e^*_{u,j}$ and $e^*_{l,j}$. Following the determination of $v^*_{s,j}$ and $v^*_{c,j}$ in the previous sections, the last term in (7) and (8) are used to calculate the upper and lower arm reference modulating signals, which are as follows:

$$e^*_{u,j} = \frac{V_{dc}}{2} - v^*_{s,j} - v^*_{c,j} \tag{30}$$

$$e^*_{l,j} = \frac{V_{dc}}{2} + v^*_{s,j} - v^*_{c,j} \tag{31}$$

The number of SMs required to be inserted into the both upper ($N_{u,j}$) and lower ($N_{l,j}$) arms can be specified by employing a particular modulation technique, like phase-shifted and level-shifted PWM or NLM as in [24].

C. MODULATION AND INNER-ARM CAPACITOR VOLTAGE BALANCING STRATEGY

The control tiers of each MMC can be categorized into high-level and low-level controllers [25]. In this paper, the low-level control involves the implementation of phase-shifted PWM (PS-PWM) and the slow-rate capacitor voltage balancing. The switching signals for each SM are produced by employing a PS-PWM method as described in [26], combined with slow-rate inner-arm capacitor voltage balancing strategy. This strategy ensures that the sorting algorithm operates at a low execution frequency as outlined in [27], thereby leading to a significant reduction in the switching frequency of the MMC. Applying the PS-PWM, which involves comparing $e^*_{u,j}$ and $e^*_{l,j}$ with N triangular carriers arranged with a phase shift of $360^\circ/N$ in each arm (no phase shift is needed between the upper and lower arm triangular carriers), resulting in terminal voltage of MMC with N + 1 voltage levels.

D. OVERALL CONTROL STRUCTURE

The overall control structure illustrating each block discussed in previous sections, as well as the proposed LMI-LQR strategy for the MMC is depicted in Fig. 2. The AC-side phase currents and circulating currents should be controlled using LMI-LQR control strategy.

It is noteworthy that achieving the reference for the circulating current involves employing an external leg-level balancing method. This method ensures that the average of 2N submodule capacitor voltages in each leg ($\bar{v}_{c,j}$) as in (32) remains constant at a specified value v^*_c (which is submodule capacitor nominal voltage (V_{dc}/N)) [28] and [29]. In other words, this method stabilizes the operation of MMC by evenly distributing the voltage among the three phase legs and generate the value for circulating current reference.

$$\bar{v}_{c,j} = 0.5\left(\frac{1}{N}\sum_{i=1}^{N} v_{c_{i,j}} + \frac{1}{N}\sum_{i=N+1}^{2N} v_{c_{i,j}}\right) \tag{32}$$

As stated by [8] and [30], second-order oscillations are present in $\bar{v}_{c,j}$. Such voltage oscillations bring additional disturbances to the reference of circulating currents. Consequently, the voltage oscillations are eliminated from the voltage control loops through the application of the notch filter (NF) depicted in Fig. 2, where its transfer function is represented as:

$$NF(s) = \frac{s^2 + \omega_n^2}{s^2 + 2\zeta\omega_n s + \omega_n^2} \tag{33}$$

where, the center angular frequency of the notch filter is denoted as $\omega_n = 2\omega_0$, the fundamental angular frequency

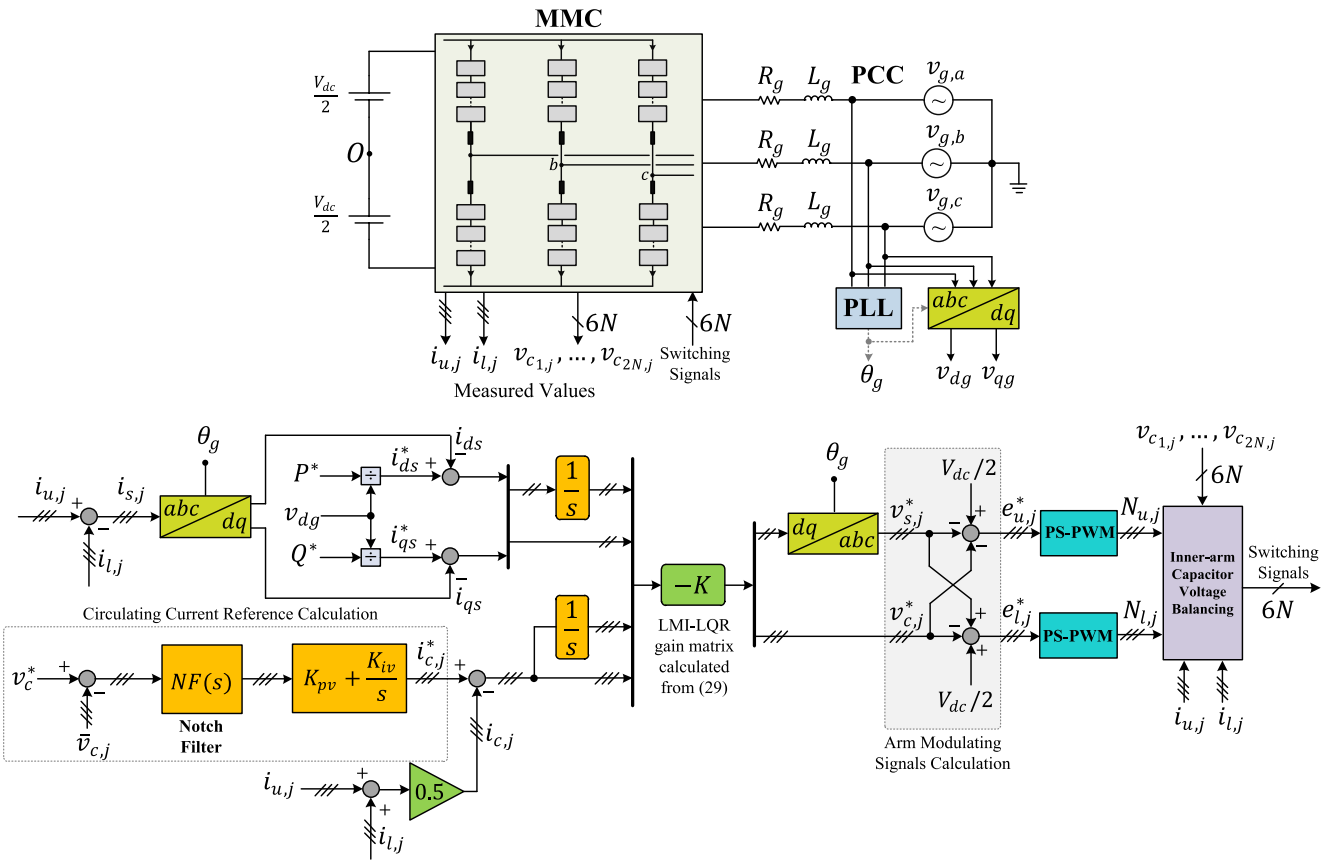

FIGURE 2. Overall control structure of MMC with the proposed LMI-LQR strategy.

is $\omega_0 = 2\pi f_0 = 120\pi$. The sharpness of the notch filter is determined by $2\zeta\omega_n$, with the damping ratio of the filter represented as ζ. The ζ is designated as 0.008. This damping ratio is related to the filter's quality factor Q, where $Q = 1/2\zeta$. Moreover, the AC-side current references are determined by the outer control loop. This paper employs a simple proportional control scheme in the outer loop to generate reference currents i^*_{ds} and i^*_{qs} for active and reactive power control. The values of i^*_{ds} and i^*_{qs} are obtained in accordance with the specified active, P^* and reactive, Q^* power references, as outlined in [31].

IV. REAL-TIME SIMULATION RESULTS

The laboratory prototype of the MMC offers valuable insights regarding the performance of the MMC. However, due to constraints, constructing a prototype of the MMC was not practical for this research. As a result, real-time simulation was utilized to analyze the performance of the MMC and the proposed control method.

In the absence of a MMC test setup, it is necessary to employ a model that emulate the performance of the MMC. The detailed switching model of MMC presents a computational challenge because the large number of devices increases the number of electrical nodes, and demands extremely small time-steps. This is particularly challenging for simulating full-scale MMC models in simulation programs, due to the increased simulation time [32] and resulting non-real-time simulation. Non-real-time or offline simulation can be avoided by either increasing the time-step or simplifying the system model [33]. To address this challenge and achieve real-time execution, this paper employs the switching function model of the MMC for real-time emulation of the MMC, as presented in [34]. It is worth noting that in the switching function model there is no requirement to compute admittance matrices, which its size increases according to the total number of nodes. Instead, all necessary numerical operations are simplified to basic integrations, multiplications, and additions [34]. At each time-step, the capacitor voltages are updated and arm voltage calculated to be applied to the controlled voltage source in each arm.

Initially, the MMC's switching function mathematical model was compared to a detailed switching model developed in MATLAB/Simulink, integrating voltage sources and both active and passive components from the SimPowerSystem library. Subsequently, due to its ability to sufficiently capture all MMC behaviors, numerical stability, and computational efficiency [34] compared to detailed switching model constructed in MATLAB/Simulink, the switching function model was implemented on the Opal-RT OP4610XG simulator for real-time emulation of the MMC.

Real-time emulation of electrical systems can be achieved through the utilization of either FPGAs or processors, with FPGAs offering expedited computation times in comparison to processors [35]. This paper utilizes a processor-based MMC model and employs the Opal-RT platform to emulate MMC dynamics and the controllers. The maximum number of SM per arm is constrained by the capacity of a single processor. On a typical processor, small MMC systems with less than 30 SM/arm can be simulated. This enables to utilize time-steps between 20 and 50 μs to attain real-time performance [36]. The MMC and the rest of the system are simulated with different sampling rates. The MMC is implemented on an Opal-RT OP4610XG simulator featuring a 3.8 GHz AMD Ryzen^{TM} processor with 6 cores, and with 10 μs time-step. The rest of the system, are simulated on the same processor with time-steps of 10 μs and 50 μs, except for sorting algorithm with greater time-step (lower execution frequency). This process decreases the computational burden on the processor, ensuring real-time implementation without overruns.

The real-time simulation platform consists of a PC and the OP4610XG target machine as the real-time simulator. Communication between the PC and the target machine is accomplished through RT-LAB 2023.1 software. The generated C code for the real-time hardware, can be loaded and executed on the Opal-RT OP4610XG after the build process.

Real-time simulation tests were conducted on a three-phase MMC connected to a stiff grid to validate and assess the effectiveness of the performance of the proposed LMI-LQR strategy. The MMC real-time simulation utilizes switching function model constructed in MATLAB/Simulink, with detailed system parameters summarized in TABLE 1. A discrete fixed-step solver is employed with a fundamental sample time of 10 μs. The nominal values of the arm resistance and inductance are provided in TABLE 1. For the calculation of the four vertices of the polytopic model for matrices A_a and B_a, a variation of $\pm 10\%$ from the nominal value is taken into account for both arm resistance and inductance. The optimization problem associated with the LMI-LQR strategy is defined in YALMIP toolbox in MATLAB environment, and then solved through the external solver MOSEK [37].

The controller performance is influenced by the weighting matrices. The weighting matrices of the performance index, Q and R, are selected through simulation evaluations of the system's transient response to ensure acceptable performance and enforcing the integral action. Therefore, the chosen Q and R matrices are as follows:

$$Q = diag\left(1, 1, 1, 1, 1, 2 \times 10^6, 10^6, 10^8, 10^8, 10^8\right) \geq 0$$
$$R = diag\,(1, 1, 1, 1, 1) > 0$$

The classical LQR controller feedback gains for the performance index in (20) and in nominal conditions can be acquired using the built-in *lqr* command in MATLAB, which is utilized as: $K = lqr(A, B, Q, R)$. Therefore, the classic

TABLE 1. System parameters.

Parameters	Value	Unit
Grid Parameters		
Rated line-to-line RMS grid voltage	4160	V
Grid fundamental frequency (f_0)	60	Hz
Grid filter inductance (L_g)	8	mH
MMC Parameters		
Rated power	1	MVA
DC-bus voltage (V_{dc})	7	kV
Arm inductance (L)	5	mH
Equivalent Arm resistance (R)	0.1	Ω
Number of submodules per arm (N)	8	---
Submodule capacitance (C)	8	mF
SM capacitor nominal voltage (V_{dc}/N)	875	V
Control Parameters		
Fundamental sample time	10	μs
Carrier frequency (f_c)	500	Hz
Leg-level balancing proportional gain (K_{pv})	3	$A.V^{-1}$
Leg-level balancing integral gain (K_{iv})	200	$A.V^{-1}.s^{-1}$

LQR controller gain matrix $K = [K_P \quad K_I]$ is as follows:

$$K_P = \begin{pmatrix} 4.464 & 0.361 & 0 & 0 & 0 \\ 0.361 & 4.371 & 0 & 0 & 0 \\ 0 & 0 & 9.950 & 0 & 0 \\ 0 & 0 & 0 & 9.950 & 0 \\ 0 & 0 & 0 & 0 & 9.950 \end{pmatrix}$$
$$K_I = \begin{pmatrix} -1065 & 657.9 & 0 & 0 & 0 \\ -930.5 & -753.1 & 0 & 0 & 0 \\ 0 & 0 & -10000 & 0 & 0 \\ 0 & 0 & 0 & -10000 & 0 \\ 0 & 0 & 0 & 0 & -10000 \end{pmatrix}$$

The robust LMI-LQR controller is derived by solving (29) within the framework of polytopic uncertainty. The resultant controller gain matrix $K = [K_P \quad K_I]$ is calculated as:

$$K_P = \begin{pmatrix} 4.494 & 0.370 & 0 & 0 & 0 \\ 0.370 & 4.415 & 0 & 0 & 0 \\ 0 & 0 & 10.648 & 0 & 0 \\ 0 & 0 & 0 & 10.648 & 0 \\ 0 & 0 & 0 & 0 & 10.648 \end{pmatrix}$$
$$K_I = \begin{pmatrix} -1058.2 & 663.5 & 0 & 0 & 0 \\ -938.4 & -748.3 & 0 & 0 & 0 \\ 0 & 0 & -10000 & 0 & 0 \\ 0 & 0 & 0 & -10000 & 0 \\ 0 & 0 & 0 & 0 & -10000 \end{pmatrix}$$

It is worth noting that there are no significant differences observed between the feedback gain matrices obtained through LMI-LQR and classic LQR control, despite that LMI optimization accounts for the uncertain MMC, whereas classic LQR control only focuses on nominal condition.

Fig. 3 depicts the calculated cost function values at the four extreme points and the optimal value offered by the calculation.

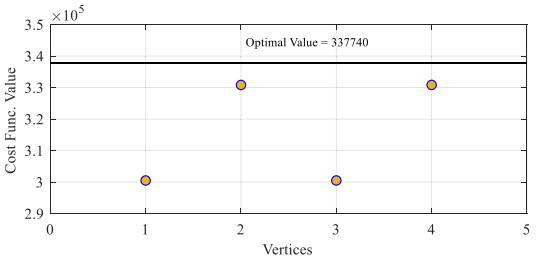

FIGURE 3. Cost function values at four extreme points and the optimal value.

To verify the proposed control approach, three cases are examined to demonstrate how the MMC system performs given the uncertainty in arm resistance and inductance parameters.

A. AC-SIDE POWER CHANGE WITHOUT UNCERTAINTY IN SYSTEM

This part investigates steady-state and dynamic performances of the MMC system when controlled by LQR and LMI-LQR strategies under nominal condition (without uncertainty in MMC system). Initially, the MMC works with no power flow, where $P^* = 0\ MW$ and $Q^* = 0\ VAR$. Then, the AC-side active power request is changed from 0 MW to 1 MW at the time of t = 1 s. Consequently, the values for i_{ds}^* and i_{qs}^* are 196.3 A and 0 A, respectively.

Fig. 4(a) depicts how i_{ds} dynamically reacts to a step change in its reference, showing that i_{ds} reaches to its reference within a timeframe of 11 ms for both methods. Moreover, the Fig. 4(b) and Fig. 4(c) illustrate that the AC-side phase current is effectively regulated using both LQR and LMI-LQR approaches. Fig. 5 illustrates the steady-state AC-side current of phase *a*. It is clear that both controllers exhibit nearly identical behavior in regulating the AC-side current. It is observed that the MMC system remains stable even during significant operation point step changes, and the transients appear smooth.

Fig. 6 illustrates the circulating current in the MMC, controlled by both LQR and LMI-LQR approaches. The result depicted in Fig. 6(a) verify that both LQR and LMI-LQR control strategies are capable of efficiently regulating the circulating current at one-third of the DC-bus current. As shown in Fig. 6(b), following the P^* step change, it requires additional time for the circulating current to settle at the new operating point. It is important to note that this seemingly sluggish response of i_c is due to the delayed update of i_c^*, which is calculated by leg-level capacitor voltage balancing method.

Fig. 7 shows the spectrum of circulating current. According to Fig. 7, the THD of the circulating current is recorded as 5.12% for the LQR and 5.02% for the LMI-LQR approach.

Moreover, Fig. 8 demonstrates that the MMC operates stable with evenly distributed voltages across the submodule capacitors in each arm when utilizing both LQR and LMI-LQR controllers as high-level controls.

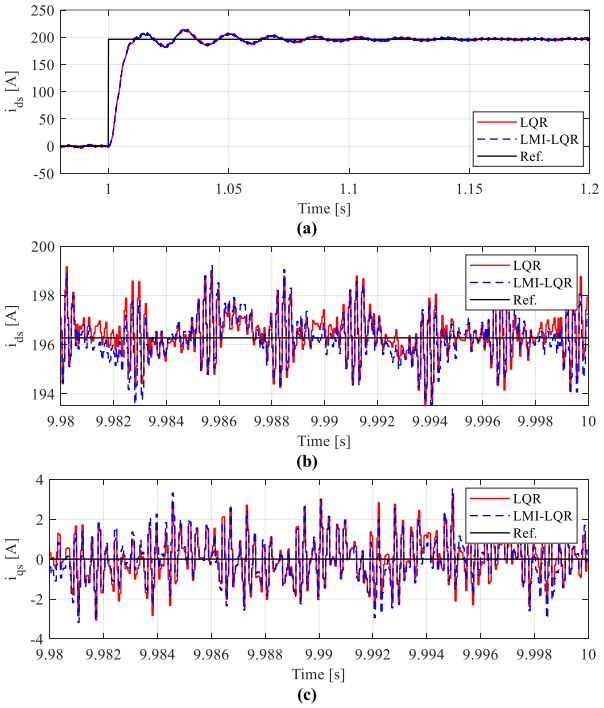

FIGURE 4. Dynamic and steady-state performance of LQR and LMI-LQR approaches under nominal condition: (a) d-axis current step response and its reference, (b) d-axis current in steady-state and its reference, (c) q-axis current in steady-state and its reference.

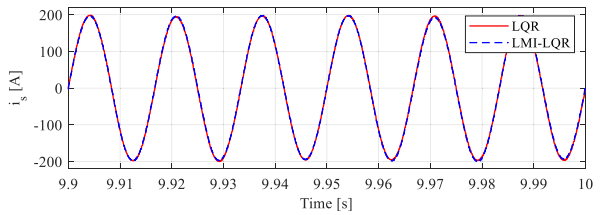

FIGURE 5. AC-side phase current of phase *a*.

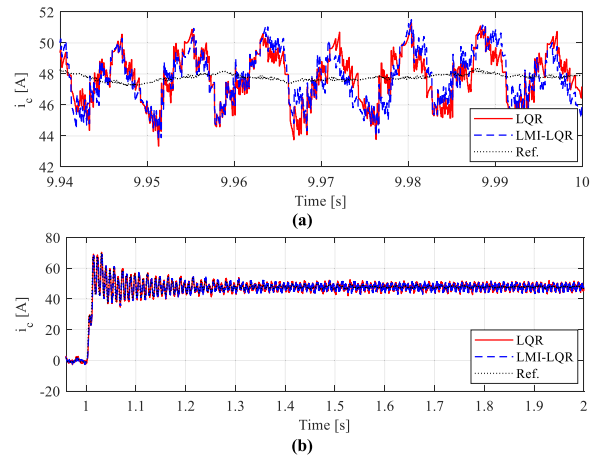

FIGURE 6. Circulating current of phase *a* and its reference: (a) Steady-state (b) Dynamic response.

B. AC-SIDE POWER CHANGE WITH UNCERTAINTY IN ARM RESISTANCE AND INDUCTANCE

In this particular case, the MMC system operates at initial operating point of zero power transfer (i.e. $P^* = 0\ MW$ and

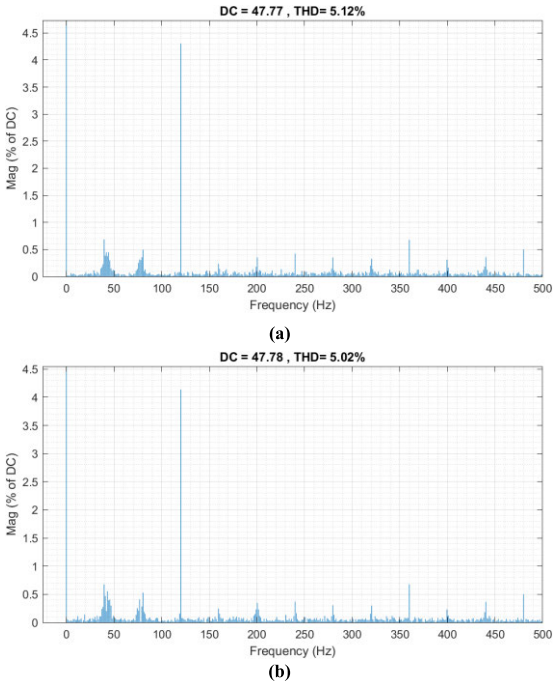

FIGURE 7. AC-side phase current spectrum: (a) LQR, (b) LMI-LQR.

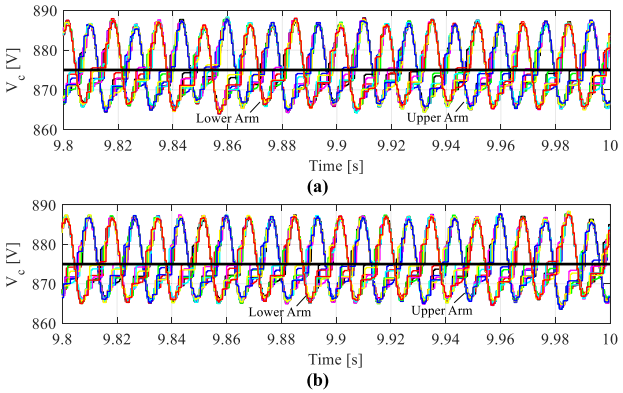

FIGURE 8. Upper arm and lower arm capacitors voltage of phase *a* in steady-state and nominal value (black line): (a) LQR, (b) LMI-LQR.

$Q^* = 0$ *VAR*). At t = 1 s, a step change in P^* occurs, changing from 0 to 1 MW.

Fig. 9 depicts the AC-side phase currents and circulating current for the MMC system under non-nominal condition, considering 10% uncertainty in arm resistance and inductance. It is notable that the derivation of gain matrix for LMI-LQR strategy incorporates 10% variation in both the R and L. Thus, robust performance is assured for arm resistance in $0.1\Omega\pm10\%$ and arm inductance between 4.5 mH and 5.5 mH. However, it is important to emphasize that such a wide variation range is used for simulation purposes and may not represent a realistic case [12]. In Fig. 9(a), it is evident that during dynamic response, the AC-side current controlled by the LQR method exceeds that of the LMI-LQR approach by approximately 3 A. However, as the system reaches steady-state, this discrepancy disappears. In Fig. 9(b), the circulating current controlled by the LMI-LQR method

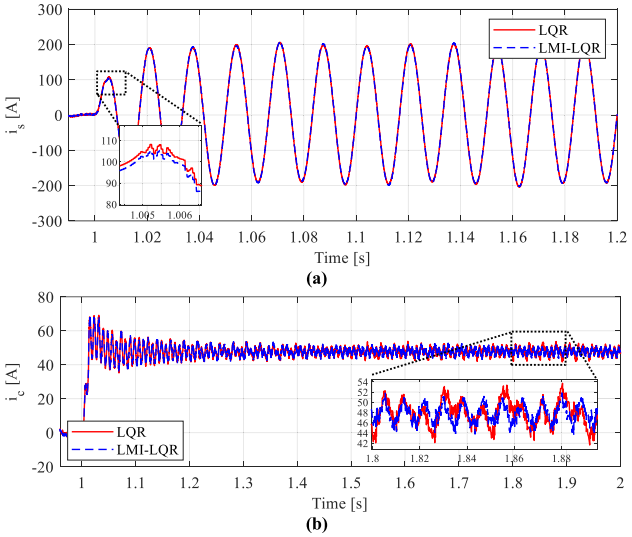

FIGURE 9. The performance of LQR and LMI-LQR approaches under non-nominal condition: (a) AC-side current of phase *a*, (b) Circulating current of phase *a*.

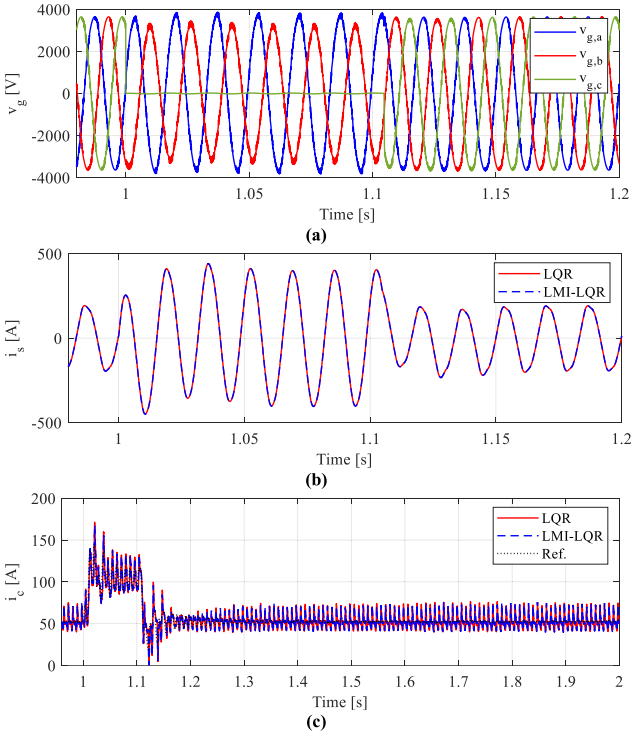

FIGURE 10. The performance of LQR and LMI-LQR approaches under single phase-to-ground fault: (a) Grid voltage (b) AC-side current of phase *a*, (c) Circulating current of phase *a*.

shows less amplitude variation in comparison to the LQR approach during steady-state.

It can be observed that the LMI-LQR method exhibits less variation in comparison to LQR method in condition where parameters are uncertain. This highlights the advantages of the LMI-LQR approach in control of the MMC with uncertain parameters.

C. SINGLE PHASE-TO-GROUND FAULT AT PCC

The aim of this investigation is to assess the effectiveness of the controllers during a temporary single-phase-to-ground fault. Prior to the fault occurrence, the MMC was operating steadily, providing 1 MW of active power and 0 VAR of reactive power. In this case in order to observe the response of controllers, it is presumed that the MMC is connected to a weak grid with an X/R ratio of 1. At t = 1 s, a phase-to-ground fault is introduced to phase *c* at the point of common coupling (PCC), lasting for 100 ms. Throughout this period, the active and reactive power set-points remained unchanged at their pre-fault values.

Fig. 10 shows the grid voltage, AC-side phase current and circulating current of phase *a* during and after temporary fault. In this case, as depicted in Fig. 10(b) and 10(c), both the LQR and LMI-LQR approaches exhibit identical behavior during and after temporary fault condition.

V. CONCLUSION

This paper proposed an LMI-based LQR approach, expanding on prior investigations into LQR control of MMCs, ensuring robust control performance under uncertain parameter conditions. The LMI-LQR controller was designed employing an augmented state-space model of the MMC. The selection of weighting matrices of the performance index was determined through simulation assessments of the transient response to ensure favorable MMC behavior. Following the selection of these matrices, the gain matrix was computed using the YALMIP toolbox for the proposed LMI-LQR method. Furthermore, this paper utilizes a processor-based MMC model and employs the Opal-RT platform to emulate MMC performance and the controller. The fully digital real-time simulation results demonstrate satisfactory dynamic and steady-state performance when the proposed controller is subjected to AC-side power variation under both nominal and non-nominal conditions, as well as during a single phase-to-ground fault at the PCC. Moreover, the proposed method exhibited more robust performance compared to the classic LQR method under condition of uncertain parameters.

REFERENCES

[1] R. Picas, J. Zaragoza, J. Pou, and S. Ceballos, "Reliable modular multilevel converter fault detection with redundant voltage sensor," *IEEE Trans. Power Electron.*, vol. 32, no. 1, pp. 39–51, Jan. 2017.

[2] G. Konstantinou, J. Pou, S. Ceballos, R. Picas, J. Zaragoza, and V. G. Agelidis, "Control of circulating currents in modular multilevel converters through redundant voltage levels," *IEEE Trans. Power Electron.*, vol. 31, no. 11, pp. 7761–7769, Nov. 2016.

[3] M. Saeedifard and R. Iravani, "Dynamic performance of a modular multilevel back-to-back HVDC system," *IEEE Trans. Power Del.*, vol. 25, no. 4, pp. 2903–2912, Oct. 2010.

[4] A. F. Cupertino, J. V. M. Farias, H. A. Pereira, S. I. Seleme, and R. Teodorescu, "Comparison of DSCC and SDBC modular multilevel converters for STATCOM application during negative sequence compensation," *IEEE Trans. Ind. Electron.*, vol. 66, no. 3, pp. 2302–2312, Mar. 2019.

[5] G. Guo, H. Wang, Q. Song, J. Zhang, T. Wang, B. Ren, and Z. Wang, "HB and FB MMC based onshore converter in series-connected offshore wind farm," *IEEE Trans. Power Electron.*, vol. 35, no. 3, pp. 2646–2658, Mar. 2020.

[6] M. A. Perez, D. Arancibia, S. Kouro, and J. Rodriguez, "Modular multilevel converter with integrated storage for solar photovoltaic applications," in *Proc. 39th Annu. Conf. IEEE Ind. Electron. Soc.*, Vienna, Austria, Nov. 2013, pp. 6993–6998.

[7] T. Soong and P. W. Lehn, "Evaluation of emerging modular multilevel converters for BESS applications," *IEEE Trans. Power Del.*, vol. 29, no. 5, pp. 2086–2094, Oct. 2014.

[8] J. Wang, X. Liu, Q. Xiao, D. Zhou, H. Qiu, and Y. Tang, "Modulated model predictive control for modular multilevel converters with easy implementation and enhanced steady-state performance," *IEEE Trans. Power Electron.*, vol. 35, no. 9, pp. 9107–9118, Sep. 2020.

[9] E. Rakhshani, K. Rouzbehi, J. M. Escaño, and J. Rueda Torres, "Optimal linear control of modular multi-level converters with a prescribed degree of stability," *Electric Power Compon. Syst.*, vol. 48, nos. 1–2, pp. 30–41, Jan. 2020.

[10] M. Jeong, S. Fuchs, and J. Biela, "High performance LQR control of modular multilevel converters with simple control structure and implementation," in *Proc. 22nd Eur. Conf. Power Electron. Appl. (EPE ECCE Europe)*, Lyon, France, Sep. 2020, pp. P.1–P.10.

[11] P. Münch, D. Görges, M. Izák, and S. Liu, "Integrated current control, energy control and energy balancing of modular multilevel converters," in *Proc. 36th Annu. Conf. IEEE Ind. Electron. Soc. (IECON)*, Glendale, AZ, USA, Nov. 2010, pp. 150–155.

[12] M. M. Belhaouane, M. Ayari, X. Guillaud, and N. B. Braiek, "Robust control design of MMC-HVDC systems using multivariable optimal guaranteed cost approach," *IEEE Trans. Ind. Appl.*, vol. 55, no. 3, pp. 2952–2963, May 2019.

[13] C. Olalla, R. Leyva, A. El Aroudi, and I. Queinnec, "Robust LQR control for PWM converters: An LMI approach," *IEEE Trans. Ind. Electron.*, vol. 56, no. 7, pp. 2548–2558, Jul. 2009.

[14] E. Feron, V. Balakrishnan, S. Boyd, and L. El Ghaoui, "Numerical methods for H_2 related problems," in *Proc. Amer. Control Conf.*, Chicago, IL, USA, Jun. 1992, pp. 1–2.

[15] X. Liu, L. Qiu, J. Rodríguez, K. Wang, Y. Li, and Y. Fang, "Learning-based neural dynamic surface predictive control for MMC," *IEEE Trans. Power Electron.*, vol. 38, no. 1, pp. 53–59, Jan. 2023.

[16] D. Weber, M. Schenke, and O. Wallscheid, "Safe reinforcement learning-based control in power electronic systems," in *Proc. Int. Conf. Future Energy Solutions (FES)*, Vaasa, Finland, Jun. 2023, pp. 1–6.

[17] D. Alfred, D. Czarkowski, and J. Teng, "Reinforcement learning-based control of a power electronic converter," *Mathematics*, vol. 12, no. 5, p. 671, Feb. 2024.

[18] B. Kedjar and K. Al-Haddad, "DSP-based implementation of an LQR with integral action for a three-phase three-wire shunt active power filter," *IEEE Trans. Ind. Electron.*, vol. 56, no. 8, pp. 2821–2828, Aug. 2009.

[19] P. Gahinet, A. Nemirovskii, A. J. Laub, and M. Chilali, "The LMI control toolbox: For Use with MATLAB," The Mathworks, Inc., May 1995.

[20] R. A. Garcia-Garcia and M. Arias-Montiel, "Linear controllers for the NXT ballbot with parameter variations using linear matrix inequalities [lecture notes]," *IEEE Control Syst. Mag.*, vol. 36, no. 3, pp. 121–136, Jun. 2016.

[21] M. Chilali and P. Gahinet, "H_∞ design with pole placement constraints: An LMI approach," *IEEE Trans. Automat. Contr.*, vol. 41, no. 3, pp. 358–367, Mar. 1996.

[22] J. Wang, R. Burgos, and D. Boroyevich, "Switching-cycle state-space modeling and control of the modular multilevel converter," *IEEE J. Emerg. Sel. Topics Power Electron.*, vol. 2, no. 4, pp. 1159–1170, Dec. 2014.

[23] S. Fuchs, S. Beck, and J. Biela, "Analysis and reduction of the output voltage error of PWM for modular multilevel converters," *IEEE Trans. Ind. Electron.*, vol. 66, no. 3, pp. 2291–2301, Mar. 2019.

[24] P. Hu and D. Jiang, "A level-increased nearest level modulation method for modular multilevel converters," *IEEE Trans. Power Electron.*, vol. 30, no. 4, pp. 1836–1842, Apr. 2015.

[25] A. Zama, S. A. Mansour, D. Frey, A. Benchaib, S. Bacha, and B. Luscan, "A comparative assessment of different balancing control algorithms for modular multilevel converter (MMC)," in *Proc. 18th Eur. Conf. Power Electron. Appl. (EPE ECCE Europe)*, Karlsruhe, Germany, Sep. 2016, pp. 1–10.

[26] A. Dekka, B. Wu, N. R. Zargari, and R. L. Fuentes, "Dynamic voltage balancing algorithm for modular multilevel converter: A unique solution," *IEEE Trans. Power Electron.*, vol. 31, no. 2, pp. 952–963, Feb. 2016.

[27] J. Qin and M. Saeedifard, "Reduced switching-frequency voltage-balancing strategies for modular multilevel HVDC converters," *IEEE Trans. Power Del.*, vol. 28, no. 4, pp. 2403–2410, Oct. 2013.
[28] M. Hagiwara, R. Maeda, and H. Akagi, "Control and analysis of the modular multilevel cascade converter based on double-star chopper-cells (MMCC-DSCC)," *IEEE Trans. Power Electron.*, vol. 26, no. 6, pp. 1649–1658, Jun. 2011.
[29] M. Zhang, L. Huang, W. Yao, and Z. Lu, "Circulating harmonic current elimination of a CPS-PWM-based modular multilevel converter with a plug-in repetitive controller," *IEEE Trans. Power Electron.*, vol. 29, no. 4, pp. 2083–2097, Apr. 2014.
[30] S. Yang, P. Wang, and Y. Tang, "Feedback linearization-based current control strategy for modular multilevel converters," *IEEE Trans. Power Electron.*, vol. 33, no. 1, pp. 161–174, Jan. 2018.
[31] A. Yazdani and R. Iravani, *Grid-Imposed Frequency VSC System: Control in dq-Frame*. Hoboken, NJ, USA: Wiley, 2010.
[32] U. N. Gnanarathna, A. M. Gole, and R. P. Jayasinghe, "Efficient modeling of modular multilevel HVDC converters (MMC) on electromagnetic transient simulation programs," *IEEE Trans. Power Del.*, vol. 26, no. 1, pp. 316–324, Jan. 2011.
[33] M. D. Omar Faruque, T. Strasser, G. Lauss, V. Jalili-Marandi, P. Forsyth, C. Dufour, V. Dinavahi, A. Monti, P. Kotsampopoulos, J. A. Martinez, K. Strunz, M. Saeedifard, X. Wang, D. Shearer, and M. Paolone, "Real-time simulation technologies for power systems design, testing, and analysis," *IEEE Power Energy Technol. Syst. J.*, vol. 2, pp. 63–73, 2015.
[34] G. P. Adam, P. Li, I. A. Gowaid, and B. W. Williams, "Generalized switching function model of modular multilevel converter," in *Proc. IEEE Int. Conf. Ind. Technol. (ICIT)*, Seville, Spain, Mar. 2015, pp. 2702–2707.
[35] A. Omar, A. Wood, H. Laird, and P. Gaynor, "Real-time emulation of a PMSM-loaded MMC with BESS," *IEEE Access*, vol. 11, pp. 55035–55045, 2023.
[36] W. Li, L.-A. Gregoire, P.-Y. Robert, S. Souvanlasy, and J. Belanger, "Modular multilevel converter model implemented in FPGA for HIL test of industrial controllers," in *Proc. IEEE PES Gen. Meeting*, National Harbor, MD, USA, Jul. 2014, pp. 1–5.
[37] J. Lofberg, "YALMIP: A toolbox for modeling and optimization in MATLAB," in *Proc. IEEE Int. Conf. Robot. Autom.*, Taiwan, Sep. 2004, pp. 284–289.

HOMA SHEIKHI JOUYBARY (Student Member, IEEE) received the B.Sc. and M.Sc. degrees in electrical engineering from the Babol Noshirvani University of Technology (BNUT), Iran, in 2012 and 2015, respectively. She is currently pursuing the joint Ph.D. degree in power electronics from Iran University of Science and Technology (IUST), Tehran, Iran, and the University of Picardie Jules Verne (UPJV), Amiens, France. Her research interests include the modeling and control of modular multilevel converters and the integration of renewable energy sources into smart grids using power converters.

AUGUSTIN MPANDA MABWE (Senior Member, IEEE) received the Ph.D. degree in electrical engineering from the University of Mons, Mons, Belgium (formerly, Mons Polytechnic Faculty), in 1990. He is currently a Professor of electrical engineering with the UniLaSalle Polytechnic Institute, France, and is heading up the Research Team on sustainable energy systems. Since 2007, he has been a Visiting Professor with the Tshwane University of Technology, Pretoria, South Africa. He is the author and co-author of many papers in international journals and conferences. He has participated in many European Union, National France, and Regional Hauts-de-France projects collaborating with European and French leading industries. His research interests include designs, modeling, and simulation of multi-phase electrical machines, power electronic converters, energy storage solutions for decarbonizing electricity generation, HVdc and FACTS, smart grids, and controls.

DAVOOD ARAB KHABURI was born in 1965. He received the B.Sc. degree in electronic engineering from the Sharif University of Technology, Tehran, Iran, in 1990, and the M.Sc. and Ph.D. degrees in electrical engineering from ENSEM, INPEL, Nancy, France, in 1994 and 1998, respectively. He joined the University of Technology of Compiègne (UTC), Compiègne, France, for one year, from 1998 to 1999. Since January 2000, he has been a Faculty Member with the Electrical Engineering Department, Iran University of Science Technology (IUST), where he is currently an Associate Professor. He is also the Head of the Power Group, IUST. He is one of the founders of Iranian Association of Power Electronics. His research interests include power electronics, motor drives, and digital control. He is currently a board member of Iranian Association of Power Electronics. He is also a member of the Center of Excellence for Power Systems Automation and Operation.

AHMED EL HAJJAJI received the Ph.D. degree in automatic control and the H.D.R. degree from the University of Picardie Jules Verne (UPJV), France, in 1993 and 2000, respectively. He was the Director of the Professional Institute of Electrical Engineering and Industrial Computing from 2006 to 2012. He is currently a Full Professor and the Head of the Automatic Control and Vehicle Research Group, Modeling Information Systems Laboratory (MIS Lab), UPJV. Since 1994, he has published more than 650 journal and conference papers in the areas of advanced fuzzy control, fault detection and diagnosis, and fault tolerant control and their applications to vehicle dynamics, engine control, power systems, renewable energy conversion systems, and industrial processes. His research interests include fuzzy control, vehicle dynamics, fault-tolerant control, neural networks, maglev systems, and renewable energy conversion systems.